Research Article

Xiaobo Liu#, Shuang Lu#, Zhen Tang*, Zhaojia Wang*, and Tianyong Huang

Removal of sulfate from aqueous solution using Mg–Al nano-layered double hydroxides synthesized under different dual solvent systems

https://doi.org/10.1515/ntrev-2021-0012
received January 13, 2021; accepted March 11, 2021

Abstract: Because of its priority to remove anions, nano-layered double hydroxide (LDH) was incorporated to improve the sulfate attack corrosion resistance of cement-based materials. Herein, the synthesis of high-efficiency LDH for removal of SO_4^{2-} is necessary. In this study, LDH with different Mg/Al ratios was synthesized under different dual solvent systems (water and ethylene glycol/ethanol/tetrapropylammonium hydroxide). Based on the adsorption experimental results, the LDH synthesized with n(Mg:Al) = 2:1 under water and ethanol solvent systems (ET2.0) exhibits the best adsorption capacity. The $d_{(003)}$ of LDH synthesized with n(Mg:Al) = 2:1 under different dual solvent systems are 0.7844, 0.7830, and 0.7946 nm, respectively. Three LDH belong to LDH-NO_3^-. The results indicated that their surface charges show obvious difference synthesized under different dual solvent systems, which leads to differences in adsorption performance. The adsorption experimental results show that ET2.0 followed pseudo second-order kinetics and Langmuir model. The ET2.0 removed SO_4^{2-} through anion substitution and electrostatic interaction and exhibited excellent adsorption rate with the maximum adsorption capacity of 95.639 mg/g. The effects of pore solution anion (OH^-, Cl^-, and CO_3^{2-}) on the removal of SO_4^{2-} by the ET2.0 are limited.

Keywords: LDH, nano-layer, adsorption capacity, corrosion resistance

1 Introduction

During the service period of concrete, temperature, load, electric field, ion erosion, *etc*. all have adverse effects on the durability of concrete, which greatly shorten the service period of concrete and cause huge safety problem [1]. In recent years, with the development of the marine construction industry, marine concrete has been widely used [2]. However, marine concrete is facing serious ion erosion problems, which has attracted widespread attention by researchers [3]. Among the erosion anions, the SO_4^{2-} does the greatest damage to concrete [4]. Incorporating mineral admixtures such as slag, fly ash, and silica fume can effectively improve the durability of cement-based materials [5]. The finer particle mineral admixtures have a certain filling effect, thereby improving the pore structure of cement-based materials [6]. Moreover, these active mineral admixtures can react with the hydration products and hinder the interaction reaction with sulfate [7]. However, the dosage of mineral admixtures is relatively large and cannot effectively solve the free SO_4^{2-} in the pore solution, which will pose a huge threat to cement-based materials. When sulfate is precipitated in the form of sodium sulfate decahydrate, it undergoes three-fold volume expansion [8]. Therefore, reducing

# Xiaobo Liu and Shuang Lu contributed equally to this work.

*** Corresponding author: Zhen Tang,** School of Civil Engineering, Harbin Institute of Technology, 150090, Harbin, China; Key Lab of Structures Dynamic Behavior and Control of the Ministry of Education, Harbin Institute of Technology, Harbin 150090, China, e-mail: tangzhenjlu@126.com
*** Corresponding author: Zhaojia Wang,** State Key Laboratory of Solid Waste Reuse for Building Materials, Beijing Building Materials Academy of Science Research, Beijing 100041, China, e-mail: wangzhaojia@bbmg.com.cn
Xiaobo Liu: Heilongjiang Province Hydraulic Research Institute, 78 Yanxing Road, Nangang District, Harbin 150080, China
Shuang Lu: School of Civil Engineering, Harbin Institute of Technology, 150090, Harbin, China; Key Lab of Structures Dynamic Behavior and Control of the Ministry of Education, Harbin Institute of Technology, Harbin 150090, China
Tianyong Huang: State Key Laboratory of Solid Waste Reuse for Building Materials, Beijing Building Materials Academy of Science Research, Beijing 100041, China

the content of SO_4^{2-} in the pore solution is a meaningful study.

Nano-layered double hydroxide (LDH) belongs to *R*-3*m* (166) space group, with the general formula of $[M^{2+}_{1-x}M^{3+}_x(OH)_2]^{x+}(A^{n-})_{x/n}\cdot mH_2O$, where M^{2+} and M^{3+} are divalent and trivalent metal cations, respectively; A^{n-} is the interlayer anion [9]. $[M(OH)_6]$ (M^{2+} or M^{3+}) octahedrons with common edges make up the positively charged layer [10]. The interlayer anions of LDH can be replaced by other anions, so LDH has been widely used to remove anions such as nitrate, phosphate, and sulfate [11]. Because of its priority to remove anions, the researchers have focused on LDH and studied the effect of LDH on the sulfate attack corrosion resistance of cement-based materials [12]. On one hand, the sulfate is solidified by adsorption, which prevents the reaction between LDH and cement hydration products [13]. On the other hand, LDH as a nano-layer material also played a role in filling and improved the pore structure of cement-based materials [14]. The existing research has carried out many studies; however, there are still some shortcomings [15]. To be specific, the synthesis of high-efficiency LDH for removal of SO_4^{2-} is rarely considered and the effect of anions that may exist in the pore solution of cement-based materials on the adsorption of SO_4^{2-} by the LDH was rarely explored. Both factors affect the ability of LDH to adsorb sulfate, which is closely related to the sulfate corrosion resistance of cement-based materials mixed with LDH.

LDH has received wide consideration in wastewater treatment because of its priority to remove anions and low cost [16]. To improve the adsorption capacity of LDH for anions, several preparation methods have been explored as follows. Puzyrnaya *et al.* explored the effect of different ratios of Mg^{2+} to Fe^{3+} on the removal of phosphate by LDH [17]; Islam and Patel studied the adsorption kinetics and thermodynamics of Zn–Al LDH to remove nitrate [18]; and Halajnia *et al.* investigated the adsorption characteristics of nitrate on Mg–Fe and Mg–Al LDH [19]. The results of these studies indicate that different cation types and the ratio of M^{2+} to M^{3+} all affect the charge of LDH, which is closely related to the anion adsorption capacity of LDH [20]. LDH removes anions through not only electrostatic interaction but also anion substitution. According to previous research results, the order of stability of interlayer inorganic anions is $CO_3^{2-} > SO_4^{2-} > OH^- > F^- > Cl^- > Br^- > NO_3^-$ [21]. For example, LDH-NO_3^- can effectively remove CO_3^{2-}; however, LDH-CO_3^{2-} is difficult to remove NO_3^-. Therefore, based on the type of anion actually adsorbed, the type of interlayer anion of LDH synthesized must be designed [22]. In addition to anions, organic matter can be intercalated with LDH to further improve its adsorption capacity. The research results of Wei *et al.* show that compared with LDH-CO_3^{2-}, LDH intercalated with aminobenzoate can more effectively remove Cl^- [23].

The morphology of LDH can also be adjusted, and LDH with a suitable morphology can expose more active sites, which is closely related to the adsorption capacity of LDH. For example, Yang *et al.* synthesized 2D nanosheet LDH by co-precipitation method, and CaFeAl LDH shows excellent adsorption capacity with the maximum chloride adsorption capacity 3.18 mmol/g [24]; Ji *et al.* prepared mesoporous MgAl LDH with the maximum bromate adsorption capacity 59.34 mg/g [25]; Hu *et al.* synthesized hierarchical CuAl LDH, which also shows excellent phosphate adsorption capacity [26]. Furthermore, because of the excellent properties of carbon materials, various composites containing carbon materials have been prepared [27,28]. Biochar-MgAl LDH nanocomposites synthesized by the co-precipitation method also show excellent adsorption capacity, and the maximum adsorption capacities of PO_4^{3-} and NO_3^- are 177.97 and 28.06 mg/g, respectively [29].

As mentioned above, compared with pristine LDH, organic cross-linked LDH and LDH composites have more active sites [30]. These active sites mainly provided by organic matter or other adsorption materials are fixed and difficult to be improved, so improving the pristine LDH adsorption capacity is important. The influence of different cation types and interlayer anions on the adsorption capacity has been extensively studied [31]. However, the maximum adsorption capacity of LDH is still limited for SO_4^{2-}, which is important for sulfate corrosion resistance of cement-based materials [32]. Herein, the synthesis of high-efficiency LDH for removal of SO_4^{2-} is necessary. In addition, the effect of anions that may exist in the pore solution of cement-based materials on the adsorption of SO_4^{2-} by the LDH is rarely considered and worthy of further exploration [33].

LDH removes anions through electrostatic interaction and anion substitution [34]. Therefore, in this study, LDH-NO_3^- was synthesized to remove sulfate based on the order of stability of interlayer inorganic anions. LDH with different Mg/Al ratios were synthesized under different dual solvent systems to adjust LDH surface charge and improve its adsorption efficiency for SO_4^{2-}. Based on adsorption test results, the best synthesis method is determined. X-ray diffractometer (XRD), Fourier transform infrared spectrometer (FT-IR), and zeta potential

were used to analyze the structure and surface charge of LDH synthesized under different dual solvent systems. Furthermore, the adsorption kinetics, isothermal adsorption, and adsorption mechanism of LDH with the best sulfate adsorption capacity were studied by adsorption experimental results, XRD and FT-IR. The effects of pH, Cl^-, and CO_3^{2-} on the adsorption of SO_4^{2-} were also explored.

2 Experiment

2.1 Synthesis process of LDH

The LDH was synthesized by the urea hydrolysis method. All chemical reagents used in this study were in accordance with the analytical grade, and the deionized water was used throughout the research. The molar ratio of $n(CO(NH_2)_2)$:$n(Mg^{2+} + Al^{3+})$ is set to be 10:1. The molar ratio of Mg:Al was 3.5:1, 3:1, 2.5:1, 2:1, and 1.5:1, respectively. To be more specific, first, 21 g $CO(NH_2)_2$, 50 mL water, and 50 mL ethanol (ET) were mixed together and corresponding mass of $Mg(NO_3)_2{\cdot}6H_2O$ and $Al(NO_3)_3{\cdot}9H_2O$ was dissolved in 100 mL deionized water. Second, two solutions were mixed and stirred at 50°C for 20 min. After stirring, the mixed solution was heated at 150°C for 12 h. Then, the precipitate was separated and washed with deionized water. Finally, the LDH-ET was dried at 100°C for 6 h. LDH-EG and LDH-TPAOH were synthesized by replacing 50 mL ethanol with 50 mL ethylene glycol (EG) or 5.3 g tetrapropylammonium hydroxide, respectively. In the dual solvent systems containing ET, the LDH with the n(Mg:Al) ratio of 2:1 was named ET2.0. The naming method for other LDHs is the same.

2.2 Batch adsorption experiments

To determine the optimal synthesis method, the removal of SO_4^{2-} by LDH with various n(Mg:Al) ratios under different dual solvent systems was studied by the batch adsorption experiments. Na_2SO_4 was used to prepare SO_4^{2-} solution in this research. The acquiescent parameters of batch adsorption experiments consist of volume (50 mL), temperature (298 K), adsorbent mass (4 g/L), initial concentration (5 mmol/L), and rotational speed (150 rpm). The sulfate concentration was tested by ion chromatography. The sulfate removal rate is determined by the following formula:

$$\%\ \text{removal rate} = (C_0 - C_e)/C_0, \quad (1)$$

where C_0 and C_e represent the initial and equilibrium concentration of SO_4^{2-}, respectively.

According to the batch adsorption experiment results, the LDH with the optimal adsorption capacity was systematically tested in subsequent adsorption experiments. First, different concentrations of Na_2SO_4 solution and LDH were mixed to investigate the adsorption isotherm of LDH on SO_4^{2-}. Then, at regular intervals (15, 30, and 60 min, *etc.*), the concentrations of Na_2SO_4 solution were tested to study adsorption kinetics of LDH on SO_4^{2-}. Finally, the influence of the presence of OH^-(pH 2–13), CO_3^{2-} (0–30 mmol/L), or Cl^- (0–30 mmol/L) on the adsorption capacity of LDH was explored.

2.3 Characterization

Bruker D8 Advance XRD was used to characterize the crystal structure of LDH. The tube pressure is 40 kV, the tube flow is 40 mA, the scanning range is 10–80°, and the step length is 0.02°. FTIR-650 was applied to record the spectra within 4,000–400 cm^{-1} of LDH using the potassium bromide tablet method. The zeta potential of LDH was determined by Zeta Potential Analyzer.

3 Results and discussion

3.1 Synthesis of LDH with various n(Mg:Al) ratios and dual solvent systems

The removal rate of SO_4^{2-} by LDH with various n(Mg:Al) ratio under different dual solvent systems has been shown in Figure 1. It can be seen from Figure 1 that the LDH with the n(Mg:Al) ratio of 2:1 exhibits the best adsorption capacity under different dual solvent systems. Among EG2.0, ET2.0 and TPAOH2.0, the ET2.0 exhibited the best adsorption capacity (92.400 mg/g). Therefore, the n(Mg:Al) ratio of 2:1 has been used to highlight the differences between LDH prepared with different dual solvent systems.

The XRD analysis results are shown in Figure 2, and the detailed values are listed in Table 1. The lattice parameters c of EG2.0, ET2.0, and TPAOH2.0 are 23.533, 23.490, and 23.838 Å, respectively. The lattice parameters a are 7.849, 7.829, and 7.909 Å, respectively. The three

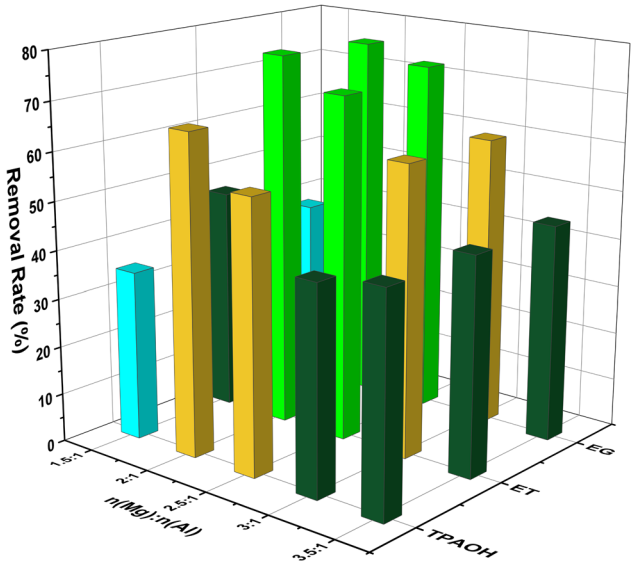

Figure 1: The removal rate of SO_4^{2-} with different LDH.

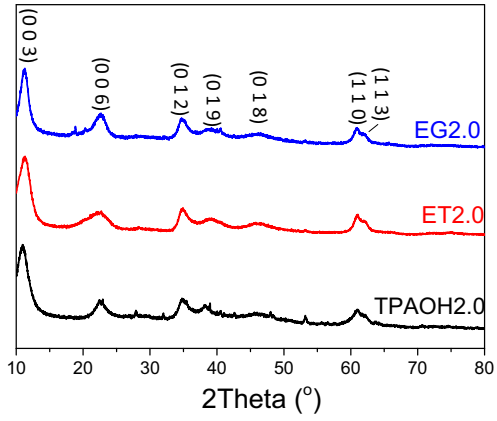

Figure 2: The XRD patterns of EG2.0, ET2.0, and TPAOH2.0.

Table 1: The interplanar spacing and lattice parameters of LDH (Å)

	$d_{(003)}$	$d_{(006)}$	$d_{(012)}$	$d_{(110)}$	c	a
EG2.0	7.844	3.925	2.585	1.519	23.533	7.849
ET2.0	7.830	3.914	2.546	1.506	23.490	7.829
TPAOH2.0	7.946	3.971	2.575	1.518	23.838	7.909

LDHs with similar lattice parameters are all hexagonal systems and belong to the *R*-3*m* (166) space group.

The FT-IR spectrum of the EG2.0, ET2.0, and TPAOH2.0 samples are presented in Figure 3. The absorption peak at around 3,465 cm^{-1} is assigned to the stretching vibrations of –OH groups [35,36]. The band at around 1,639 cm^{-1} is related to the angular deformation of water molecules [37]. The absorption peak at around 476 cm^{-1} corresponds

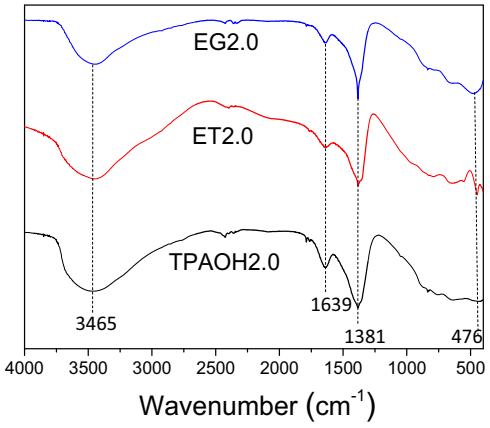

Figure 3: The FT-IR spectrum of EG2.0, ET2.0, and TPAOH2.0.

to the M–O band, and the M represents the existence of Mg or Al [38]. The absorption peak at around 1,380 cm^{-1} is associated with the NO_3^- of NO_3-LDH [39]. Therefore, it can be concluded that the three LDHs prepared are all NO_3-LDH. Moreover, there is little difference in crystal structures and functional groups of three LDHs from the results of FT-IR analysis, which is consistent with the XRD analysis results as above.

The positive and negative zeta potential corresponds to the positive and negative surface charge of LDH, which is closely related to the adsorption capacity of LDH to SO_4^{2-} [40]. LDH with positive surface charge can adsorb SO_4^{2-} by electrostatic action. The results of zeta potentials of EG2.0, ET2.0, and TPAOH2.0 samples subjected to different pH values are shown in Figure 4. When the solutions containing LDH are weakly alkaline, the zeta potentials of EG2.0 and ET2.0 are similar, and both are greater than TPAOH2.0, which leads mainly to the difference between the three LDH adsorption capacities.

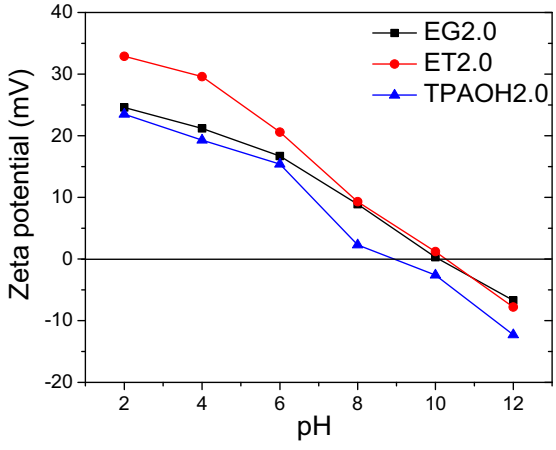

Figure 4: The zeta potential of EG2.0, ET2.0, and TPAOH2.0.

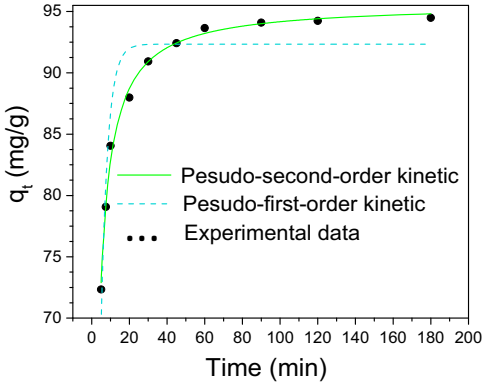

Figure 5: Adsorption kinetics of SO_4^{2-} adsorption by ET2.0.

The three crystal structures are not significantly different under different dual solvent systems. The $d_{(003)}$ of EG2.0, ET2.0, and TPAOH2.0 are 0.7844, 0.7830, and 0.7946 nm, respectively. The different nano-layer spacing has no obvious effect on the adsorption properties. However, their surface charges and system stability have certain differences, indicating that the zeta potential of LDH is positively correlated with the adsorption properties. Among EG2.0, ET2.0, and TPAOH2.0, ET2.0 has the best adsorption performance. Therefore, we have launched a systematic research on ET2.0.

3.2 Sulfate adsorption kinetics and isotherms

As shown in Figure 5, the adsorption kinetic experimental results show that SO_4^{2-} adsorption capacity by ET2.0 increased rapidly with time. Within 1 h, the adsorption capacity increased rapidly and reached 93.650 mg/g, which is very close to the maximum adsorption capacity. Kinetic simulation of the adsorption process is used to characterize the variation of adsorption capacity with time under certain temperature conditions. Commonly used adsorption kinetic models are pseudo first-order kinetics and pseudo second-order kinetics. Two equations were expressed as follows:

$$\ln(q_e - q_t) = \ln q_e - k_1 t, \tag{2}$$

$$\frac{t}{q_t} = \frac{1}{k_2 q_e^2} + \frac{t}{q_e}, \tag{3}$$

where k_1 (min^{-1}) and k_2 [g/(mg min)] are the adsorption rate constant, respectively; q_e and q_t (mg/g) represent the adsorption capacity at equilibrium and time t, respectively.

The correlation coefficient (R^2) of pseudo first-order kinetics and pseudo second-order kinetics is 0.8920 and 0.9936, respectively. It can be seen from Figure 5 that pseudo second-order kinetics equation can better fit the experimental data. The adsorption capacity (q_e = 95.639 mg/g) calculated by pseudo second-order kinetics equation is close to the experimental results. This could be explained that the adsorption rate is controlled by the chemisorption mechanism, which involves chemical reactions, electron gain and loss, or electron sharing [41,42]. This indicates that LDH removes anions mainly through anion substitution.

When the adsorption reaches equilibrium at a constant temperature, the concentration of adsorbate on the surface of the adsorbent and in the solution is distributed according to a certain rule. There is a certain functional relationship, and this relationship is called

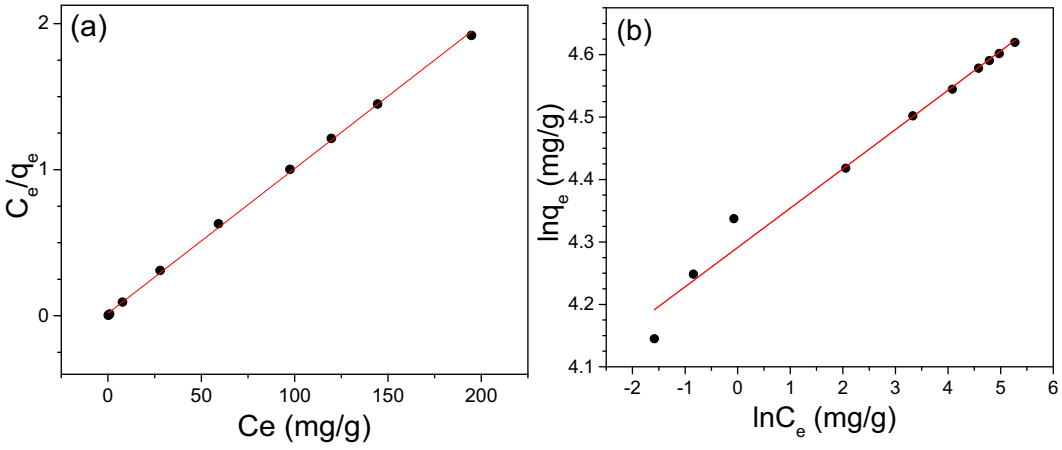

Figure 6: Adsorption isotherms of SO_4^{2-} adsorption by ET2.0 of (a) Langmuir and (b) Freundlich.

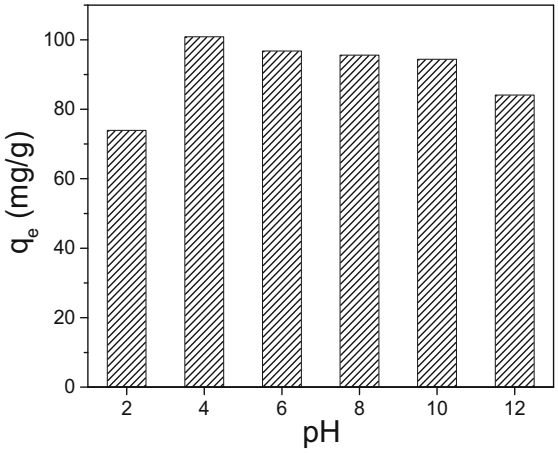

Figure 7: Effect of pH on the adsorption of SO_4^{2-} by the ET2.0.

the adsorption isotherm. Two common adsorption models Langmuir and Freundlich are as follows:

$$q_e = q_m \frac{K_L C_e}{1 + K_L C_e}, \tag{4}$$

$$q_e = K_F C_e^{\frac{1}{n}}, \tag{5}$$

where q_e (mg/g) is the adsorption capacity at equilibrium, q_m (mg/g) is the saturation absorptive capacity, C_e (mg/L) is the concentration of adsorbate at equilibrium, K_L (L/mg) is the Langmuir adsorption constant, and K_F and n represent Freundlich adsorption coefficient and adsorption intensity characteristic constant, respectively.

The fitting results of the two models are shown in Figure 6. The correlation coefficient (R^2) of Langmuir and Freundlich model is 0.9992 and 0.9778, respectively. Therefore, the Langmuir model is more suitable to describe the adsorption process of ET2.0. The basic assumption of the Langmuir adsorption isotherm model is a monolayer adsorption [43]. The number of adsorption sites is fixed, the energy of each adsorption site is the same, each adsorption site adsorbs only one molecule, and there is no interaction between them [44–46].

3.3 Effect of the solution pH

To explore adsorption mechanism and the possibility of ET2.0 applied to cement-based materials, the effect of pH on the adsorption of SO_4^{2-} by the ET2.0 was investigated. As shown in Figure 7, with the decrease in pH value, the adsorption capacity of ET2.0 to sulfate and zeta potential increases, which indicates ET2.0 can remove SO_4^{2-} by electrostatic interaction. However, when the pH value changed from 4 to 2, the adsorption capacity of ET2.0 suddenly dropped from 100.899 to 73.955 mg/g. This may be because of the crystal structure of ET2.0 changed when the pH was too low. When the pH is 12, the maximum adsorption capacity of ET2.0 to sulfate is 84.08 mg/g. It can be concluded that ET2.0 still has a good ability to remove sulfate ions under alkaline conditions and shows great potential to be applied to cement-based materials.

3.4 Adsorption mechanism

XRD and FT-IR of ET2.0 and ET2.0-SO_4^{2-} (before and after the adsorption of SO_4^{2-}) were tested to figure out the adsorption mechanism of ET2.0. As shown in Figure 8a, the crystal interplanar spacing of (003), (006), (012), (019), *etc.* of ET2.0 was not changed after removing SO_4^{2-}, indicating that the crystal structure of ET2.0 was not changed. However, there are some differences

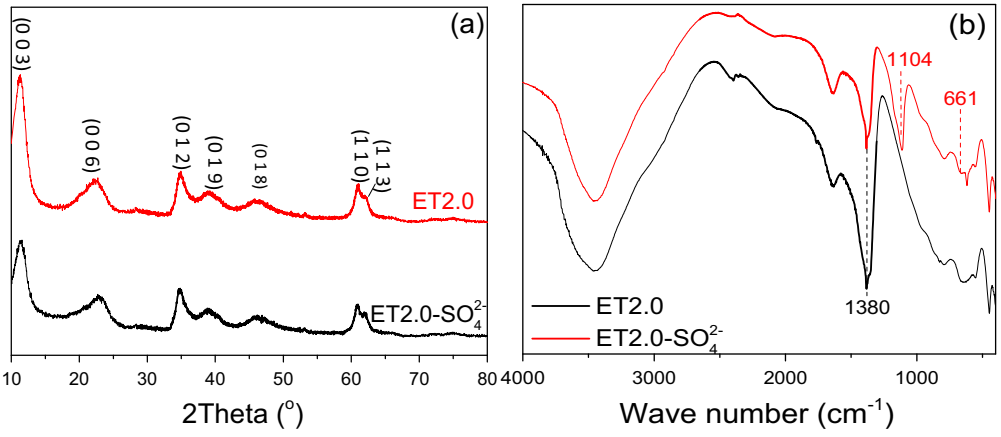

Figure 8: (a) XRD and (b) FT-IR of ET2.0 and ET2.0-SO_4^{2-}.

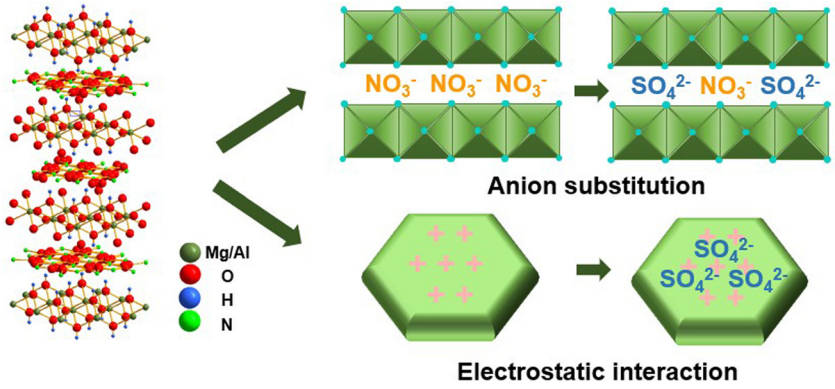

Figure 9: The schematical mechanism of the adsorption effect.

between ET2.0 and ET2.0-SO_4^{2-} as exhibited in Figure 8b. Compared with ET2.0, ET2.0-SO_4^{2-} presents the weaker absorption peaks at 1,380 cm^{-1} and two new adsorption peaks at around 1,104 and 661 cm^{-1} occur. The adsorption peaks at 1,104 and 661 cm^{-1} are related to the existence of SO_4^{2-} [47]. The weaker absorption peaks at around 1,380 cm^{-1} suggest the replace effect between SO_4^{2-} and NO_3^-, but because of the steric hindrance, NO_3^- was not completely replaced by SO_4^{2-} during the adsorption process. The adsorption capacity of ET2.0 changes with the change of pH value, which indicate ET2.0 removes SO_4^{2-} through electrostatic interaction. Combined with the above analysis, the schematic diagram of the adsorption mechanism is shown in Figure 9, it has clearly demonstrated that ET2.0 removes SO_4^{2-} through anion substitution and electrostatic interaction.

3.5 Effect of competing ions

Concrete may face different carbonization and corrosion problem during the service duration. In addition to SO_4^{2-} and OH^-, the pore solution of concrete may contain Cl^- and CO_3^{2-}. Therefore, it is necessary to investigate the effect of Cl^- and CO_3^{2-} on the adsorption of SO_4^{2-} by the ET2.0. The effect of Cl^- on the adsorption of SO_4^{2-} by the ET2.0 is shown in Figure 10a, and it can be seen that the effect of Cl^- is limited. Even when the concentration of Cl^- is six times that of SO_4^{2-}, the adsorption capacity of ET2.0 to sulfate is still above 90 mg/g. However, the CO_3^{2-} has an obvious effect on the adsorption of SO_4^{2-} by the ET2.0. As shown in Figure 10b, with the increase in concentration of CO_3^{2-}, the adsorption capacity of ET2.0 to SO_4^{2-} decreases significantly. When the CO_3^{2-}

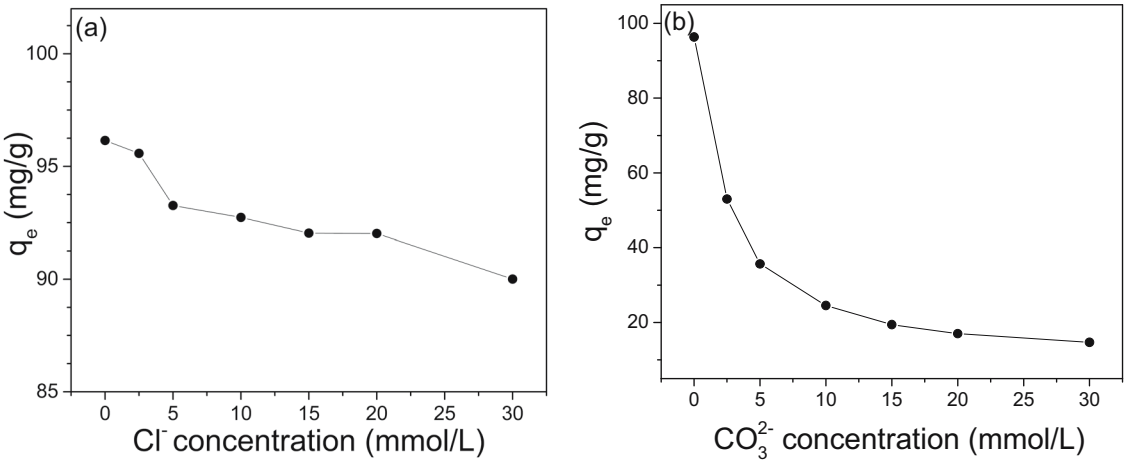

Figure 10: Effect of (a) Cl^- and (b) CO_3^{2-} on the adsorption of SO_4^{2-} by the ET2.0.

concentration is 30 mmol/L, the adsorption capacity of ET2.0 to SO_4^{2-} is only 14.68 mg/g. Moreover, in the actual pore solution, because of the presence of Ca^{2+}, the CO_3^{2-} concentration is less than 2.5 mmol/L. Therefore, the effect of CO_3^{2-} on the adsorption of SO_4^{2-} by the ET2.0 is limited in pore solution. The above conclusions indicate that ET2.0 can be used to improve the sulfate corrosion resistance of cement-based materials.

4 Conclusion

In this study, high-efficiency LDH was synthesis by urea hydrolysis method under different dual solvent systems. According to the experimental results, the following conclusions can be drawn:

(1) The LDH with the *n*(Mg:Al) ratio of 2:1 exhibited the best adsorption capacity under different dual solvent systems. Among EG2.0, ET2.0 and TPAOH2.0, the ET2.0 exhibited the best adsorption capacity (92.400 mg/g).
(2) The crystal structure and functional groups of EG2.0, ET2.0, and TPAOH2.0 showed little difference; however, the zeta potentials of EG2.0 and ET2.0 are greater than TPAOH2.0, which leads to the difference between the three LDH adsorption capacity.
(3) The adsorption kinetics and isothermal adsorption model of ET2.0 followed pseudo second-order kinetics and Langmuir model, respectively. The ET2.0 removed SO_4^{2-} through anion substitution and electrostatic interaction and exhibited excellent adsorption rate with the maximum adsorption capacity calculated of 95.639 mg/g.
(4) The effects of pore solution anion (OH^-, Cl^-, and CO_3^{2-}) on the removal of SO_4^{2-} by the ET2.0 are limited, indicating that ET2.0 can be used to improve the sulfate corrosion resistance of cement-based materials. Related research will be carried out in the future.

Funding information: This research was funded by the "National Natural Science Foundation of China" No. 51872064. This research was also supported by "State Key Laboratory of Solid Waste Reuse for Building Materials" SWR-2020-005.

Author contributions: All authors have accepted responsibility for the entire content of this manuscript and approved its submission.

Conflict of interest: The authors state no conflict of interest.

References

[1] Reiterman P, Holcapek O, Zobal O, Keppert M. Freeze-thaw resistance of cement screed with various supplementary cementitious materials. Rev Adv Mater Sci. 2019;58(1):66–74.
[2] Melchers RE, Chaves IA. Durability of reinforced concrete bridges in marine environments. Struct Infrastruct Eng. 2020;16(1):169–80.
[3] Wang J, Xu Y, Wu X, Zhang P, Hu S. Advances of graphene- and graphene oxide-modified cementitious materials. Nanotechnol Rev. 2020;9(1):465–77.
[4] Lorente S, Yssorche-Cubaynes M-P, Auger J. Sulfate transfer through concrete: Migration and diffusion results. Cem Concr Compos. 2011;33(7):735–41.
[5] Hassani MS, Asadollahfardi G, Saghravani SF. Durability and morphological assessment of concrete manufactured with sewage. Constr Build Mater. 2020;264:120202.
[6] Noushini A, Castel A, Aldred J, Rawal A. Chloride diffusion resistance and chloride binding capacity of fly ash-based geopolymer concrete. Cem Concr Compos. 2020;105:103290.
[7] Ye H, Chen Z, Huang L. Mechanism of sulfate attack on alkali-activated slag: The role of activator composition. Cem Concr Res. 2019;125:105868.
[8] Nadelman EI, Kurtis KE. Durability of Portland-limestone cement-based materials to physical salt attack. Cem Concr Res. 2019;125:105859.
[9] Sun H, Heo Y-J, Park J-H, Rhee KY, Park S-J. Advances in layered double hydroxide-based ternary nanocomposites for photocatalysis of contaminants in water. Nanotechnol Rev. 2020;9(1):1381–96.
[10] Tang Z, Qiu Z, Lu S, Shi X. Functionalized layered double hydroxide applied to heavy metal ions absorption: a review. Nanotechnol Rev. 2020;9(1):800–19.
[11] Puzyrnaya LN, Shunkov VS, Pshinko GN, Demutskaya LN, Kosorukov AA. The impact of the Mg(II)/Fe(III) ratio in the composition of layered double hydroxides for the removal of phosphate–ions from water media. J Water Chem Technol. 2018;40(4):190–5.
[12] Ke X, Bernal SA, Provis JL. Uptake of chloride and carbonate by Mg–Al 6and Ca–Al layered double hydroxides in simulated pore solutions of alkali-activated slag cement. Cem Concr Res. 2017;100:1–13.
[13] Ma J, Wang D, Duan P, Shi Y. Sulfate ions immobilization of calcined layered double hydroxides in hardened cement paste and concrete. J Wuhan Univ Technol-Mater Sci Ed. 2019;34(6):1400–7.
[14] Wu Y, Duan P, Yan C. Role of layered double hydroxides in setting, hydration degree, microstructure and compressive strength of cement paste. Appl Clay Sci. 2018;158:123–31.
[15] Mir ZM, Bastos A, Hoeche D, Zheludkevich ML. Recent advances on the application of layered double hydroxides in concrete-a review. Materials. 2020;13(6):24.
[16] Zubair M, Ihsanullah I, Aziz HA, Ahmad MA, Al-Harthi MA. Sustainable wastewater treatment by biochar/layered double hydroxide composites: progress, challenges, and outlook. Bioresour Technol. 2021;319:124128.
[17] Puzyrnaya LN, Shunkov VS, Pshinko GN, Demutskaya LN, Kosorukov AA. The impact of the Mg(II)/Fe(III) ratio in the composition of layered double hydroxides for the removal of

phosphate-ions from water media. J Water Chem Technol. 2018;40(4):190–5.
[18] Islam M, Patel R. Synthesis and physicochemical characterization of Zn/Al chloride layered double hydroxide and evaluation of its nitrate removal efficiency. Desalination. 2010;256(1–3):120–8.
[19] Halajnia A, Oustan S, Najafi N, Khataee AR, Lakzian A. The adsorption characteristics of nitrate on Mg–Fe and Mg–Al layered double hydroxides in a simulated soil solution. Appl Clay Sci. 2012;70:28–36.
[20] Hibino T. Anion selectivity of layered double hydroxides: effects of crystallinity and charge density. Eur J Inorg Chem. 2018;2018(6):722–30.
[21] Zubair M, Daud M, McKay G, Shehzad F, Al-Harthi MA. Recent progress in layered double hydroxides (LDH)-containing hybrids as adsorbents for water remediation. Appl Clay Sci. 2017;143:279–92.
[22] Xu J, Song Y, Tan Q, Jiang L. Chloride absorption by nitrate, nitrite and aminobenzoate intercalated layered double hydroxides. J Mater Sci. 2017;52(10):5908–16.
[23] Wei J, Xu J, Mei Y, Tan Q. Chloride adsorption on aminobenzoate intercalated layered double hydroxides: kinetic, thermodynamic and equilibrium studies. Appl Clay Sci,. 2020;187:105495.
[24] Yang L, Chen M, Lu Z, Huang Y, Wang J, Lu L, et al. Synthesis of CaFeAl layered double hydroxides 2D nanosheets and the adsorption behaviour of chloride in simulated marine concrete. Cem Concr Compos. 2020;114:103817.
[25] Ji H, Wu W, Li F, Yu X, Fu J, Jia L. Enhanced adsorption of bromate from aqueous solutions on ordered mesoporous Mg–Al layered double hydroxides (LDHs). J Hazard Mater. 2017;334:212–22.
[26] Hu F, Wang M, Peng X, Qiu F, Zhang T, Dai H, et al. High-efficient adsorption of phosphates from water by hierarchical CuAl/biomass carbon fiber layered double hydroxide. Colloids Surf A Physicochem Eng Asp. 2018;555:314–23.
[27] Lu H, Yao Y, Huang WM, Leng J, Hui D. Significantly improving infrared light-induced shape recovery behavior of shape memory polymeric nanocomposite via a synergistic effect of carbon nanotube and boron nitride. Compos Part B-Eng. 2014;62:256–61.
[28] Lu H, Yao Y, Huang WM, Hui D. Noncovalently functionalized carbon fiber by grafted self-assembled graphene oxide and the synergistic effect on polymeric shape memory nanocomposites. Compos Part B-Eng. 2014;67:290–5.
[29] Alagha O, Manzar MS, Zubair M, Anil I, Mu'azu ND, Qureshi A. comparative adsorptive removal of phosphate and nitrate from wastewater using biochar-MgAl LDH nanocomposites: coexisting anions effect and mechanistic studies. Nanomaterials (Basel). 2020;10(2):336.
[30] Hong SP, Yoon H, Lee J, Kim C, Kim S, Lee J, et al. Selective phosphate removal using layered double hydroxide/reduced graphene oxide (LDH/rGO) composite electrode in capacitive deionization. J Colloid Interface Sci. 2020;564:1–7.
[31] Lv LA, He J, Wei M, Evans DG, Duan X. Uptake of chloride ion from aqueous solution by calcined layered double hydroxides: equilibrium and kinetic studies. Water Res. 2006;40(4):735–43.
[32] Halajnia A, Oustan S, Najafi N, Khataee AR, Lakzian A. Adsorption–desorption characteristics of nitrate, phosphate and sulfate on Mg–Al layered double hydroxide. Appl Clay Sci. 2013;80–81:305–12.
[33] Yang B, Liu D, Lu J, Meng X, Sun Y. Phosphate uptake behavior and mechanism analysis of facilely synthesized nanocrystalline Zn–Fe layered double hydroxide with chloride intercalation. Surf Interface Anal. 2018;50(3):378–92.
[34] Lv L, Sun P, Gu Z, Du H, Pang X, Tao X, et al.Removal of chloride ion from aqueous solution by ZnAl–NO_3 layered double hydroxides as anion-exchanger. J Hazard Mater. 2009;161(2–3):1444–9.
[35] Chi L, Wang Z, Sun Y, Lu S, Yao Y. Crystalline/amorphous blend identification from cobalt adsorption by layered double hydroxides. Mater (Basel). 2018;11(9):1706.
[36] Wu Y, Chi Y, Bai H, Qian G, Cao Y, Zhou J, et al. Effective removal of selenate from aqueous solutions by the Friedel phase. J Hazard Mater. 2010;176(1–3):193–8.
[37] Yu S, Liu Y, Ai Y, Wang X, Zhang R, Chen Z, et al. Rational design of carbonaceous nanofiber/Ni–Al layered double hydroxide nanocomposites for high-efficiency removal of heavy metals from aqueous solutions. Environ Pollut. 2018;242(Pt A):1–11.
[38] Jawad A, Peng L, Liao Z, Zhou Z, Shahzad A, Ifthikar J, et al. Selective removal of heavy metals by hydrotalcites as adsorbents in diverse wastewater: different intercalated anions with different mechanisms. J Clean Prod. 2019;211:1112–26.
[39] Ma L, Wang Q, Islam SM, Liu Y, Ma S, Kanatzidis MG. Highly selective and efficient removal of heavy metals by layered double hydroxide intercalated with the $MOS_4(2-)$ ion. J Am Chem Soc. 2016;138(8):2858–66.
[40] Iftekhar S, Kucuk ME, Srivastava V, Repo E, Sillanpaa M. Application of zinc-aluminium layered double hydroxides for adsorptive removal of phosphate and sulfate: equilibrium, kinetic and thermodynamic. Chemosphere. 2018;209:470–9.
[41] Huang D, Liu C, Zhang C, Deng R, Wang R, Xue W, et al. Cr(VI) removal from aqueous solution using biochar modified with Mg/Al-layered double hydroxide intercalated with ethylenediaminetetraacetic acid. Bioresour Technol. 2019;276:127–32.
[42] Zhu D, Zuo J, Jiang Y, Zhang J, Zhang J, Wei C. Carbon-silica mesoporous composite in situ prepared from coal gasification fine slag by acid leaching method and its application in nitrate removing. Sci Total Env. 2020;707:136102.
[43] Zhao D, Wang Z, Lu S, Shi X. An amidoxime-functionalized polypropylene fiber: competitive removal of Cu(II), Pb(II) and Zn (II) from wastewater and subsequent sequestration in cement mortar. J Clean Prod. 2020;274:123049.
[44] Chi L, Wang Z, Sun Y, Lu S, Yao Y. Removal of cobalt ions from waste water by Friedel's salt. Mater Res Express. 2018;6(1):015508.
[45] Yang X, Xu Y, Xue B, Jiang Y, Li F. Cordierite reinforced graphite nanocomposite with superior adsorption capacity synthesized by in-situ carbon-bed pyrolysis method. Microporous Mesoporous Mater. 2018;265:219–26.
[46] Zhu D, Miao S, Xue B, Jiang Y, Wei C. Effect of coal gasification fine slag on the physicochemical properties of soil. Water Air Soil Pollut. 2019;230(7):155.
[47] Yang B, Dong Y, Wang BN, Yang M, Yang C. A mild alcohol-salt route to synthesize α-hemihydrate gypsum microrods from flue gas desulfurization gypsum in large scale. Mater Res Express. 2019;6(4):045507.